Rapid and Complete Prediction of Alizarin in Solution by Combining Experimental Data with Computational Methods

Thanh Huyen Linh Tran, Baptiste Rigaud, Maguy Jaber, Romain Berraud-Pache

Thanh Huyen Linh Tran, Baptiste Rigaud, Maguy Jaber, Romain Berraud-Pache. Rapid and Complete Prediction of Alizarin in Solution by Combining Experimental Data with Computational Methods. Dyes and Pigments, In press, 10.1016/j.dyepig.2024.112242 . hal-04586447

HAL Id: hal-04586447
https://hal.science/hal-04586447v1

Submitted on 29 May 2024

Rapid and Complete Prediction of Alizarin in Solution by Combining Experimental Data with Computational Methods

Thanh Huyen Linh TRAN[a], Baptiste RIGAUD[b], Maguy JABER[a,c], Romain BERRAUD-PACHE[a*]

[a] Laboratoire d'Archéologie Moléculaire et Structurale (LAMS), Sorbonne Université, CNRS, UMR 8220, Paris, 75005, France
[b] Fédération de Chimie des Matériaux de Paris-Centre FCMat
[c] IUF-Institut Universitaire de France, Paris, France
[*]corresponding author: romain.berraud-pache@sorbonne-universite.fr

ARTICLE INFO

Keywords: Computational chemistry, organic dyes, cultural heritage, UV-Vis spectrum, NMR, color prediction, solvation model

ABSTRACT

In the field of cultural heritage, understanding the nature of pigments and dyes is of great importance for conservation issues. Among the many natural dyes used in paintings or textiles, madder was one of the most important sources of red color at the time and was present in a wide variety of objects. However, due to extraction challenges, impurities, and high costs, a lot of information are not easily available. In this publication we designed a computational protocol able to reproduce the spectroscopic properties of two dyes, alizarin and alizarin red S. This framework allows us to compute both Ultraviolet-Visible absorption spectra and Nuclear Magnetic Resonance (NMR) with good accuracy as well as reproduce with precision the CIELAB color. We have also explored different types of interactions that impact these properties, notably the solvation effect. We found that microsolvation is sufficient to reproduce the experimental measurements made in water. The high accuracy of the computation method makes this technique particularly promising for a non-destructive study of dyes on works of art and the preservation of cultural heritage.

INTRODUCTION

The analytical investigation of dyes is considered of utmost importance in the field of cultural heritage. Indeed, through the identification of the corresponding dye, we are often able to gain insight into several important aspects: the characterization of the dye and the artist's techniques, the degradation pathways, the preservation state of the artifact, the dating and the determination of the provenance of objects [1–4]. Furthermore, it provides precious details to plan correct restoration, conservation, and display strategy in museums and art galleries.

Both traditional and cutting-edge techniques such as ultraviolet-visible (UV-Vis), infrared (IR), and Raman spectroscopies, as well as nuclear magnetic resonance (NMR), mass spectrometry (MS), liquid chromatography, Fiber Optics Reflectance Spectra (FORS), X-Ray diffraction (XRD) or hyperspectral spectroscopy have been reported for the analytical investigation of dyes [2,5–14]. While the accuracy and sensitivity of these techniques have allowed researchers to gain a huge amount of insight into these systems, most of the technologies are sampling-based and need complex dye extraction and chemical preparation methods. Moreover, sample collection, preparation, and chemical analysis are often challenging due to material complexity, limited sample sizes, dye degradation, and lack of appropriate standards needed for UV-Vis detection [8,15–19]. Therefore, the identification of historical dyes is still one of the most challenging tasks in the realm of heritage preservation. In this context, computational methods have emerged as an appealing tool to decipher complex experimental data [20]. These theoretical methods aid in the interpretation of individual contributions to the experimental spectrum. Unfortunately, their application in the field of cultural heritage is not as widespread as other fields of research (such as catalysis, astrochemistry, electrochemistry, etc).

Representing one of the most famous natural dyes since antiquity, madder was selected as the focus of this study [21–23]. From the roots of this plant, around 36 red colorants derivating from the anthraquinone family can be extracted in various quantities. We will focus here on alizarin, one of the main constituents of madder [24,25].

In order to study the associated dyes, the combination of NMR with UV-Vis is often used in the heritage science field because of their complementary nature. While UV-Vis is good at characterizing the environmental effect of the dye or its degradation (color fading), NMR can differentiate analog molecules. It is also very precise in attesting chemical modifications, notably when lake or pigment structures are created by association of a colored dye with a metallic ion.

For the computation of spectroscopic properties, density functional theory (DFT) and Time Dependent-DFT are often the methods of choice due to their reasonable costs and good precision. In fact, there have been many reports regarding the prediction of Alizarin color and properties using these methods [26–37]. Still, the role of the environment is not clearly understood or deciphered. Furthermore, some key properties like reproducing the UV-Vis or NMR spectra are not always present.

When examining molecules using spectroscopic analysis, a significant portion of their observable characteristics displays varying degrees of sensitivity to the surrounding environment (solvent, pH, binding partners, mordant, substrate, temperature, light, etc) [38,39]. This influence of the solvent on spectroscopic properties arises from multiple factors such as the polarity of the solvent or the presence of hydrogen bonds. It is therefore crucial to find the optimal solvation model in order to correctly predict the UV-Vis spectrum or other properties of these organic molecules.

In this study, our attention will be directed toward the impact of solvents on a precious dye, alizarin. The aim is to introduce a holistic computational protocol designed to predict color and chemical properties, developed through a collaborative effort with experimental data. The protocol integrates multiple facets, including the exploration of conformers and deprotonated forms, effective selection of optimal solvation models based on the solute-solvent system of study (implicit, microsolvated, or multilevel), prediction of UV-Vis spectrum, color prediction with CIELAB coordinates and ^{13}C and ^{1}H NMR shift predictions. This protocol will be applied to two dyes: alizarin and alizarin red S.

1. MATERIALS & METHODS

2.1. EXPERIMENTAL METHOD

UV Spectrum

Alizarin (97% purity) was purchased from Sigma Aldrich and used without further purification. Alizarin red S pure (sodium alizarinsulfonate) was purchased from Thermoficher.

10 mg of alizarin were dissolved in 40 mL of deionized water (MilliQ). The alizarin solution was then heated for 2 hours at 90°C, and filtered using a Buchner funnel. 5mg of alizarin red S was added to 80 mL of distilled water and stirred for 10min. The obtained solution was used directly without heating or filtering. Then, the pH was adjusted using either hydrochloric acid (HCl, 0.1M) or sodium hydroxide (NaOH, 1M). Three pH values were considered for alizarin (pKa_1=5.5 and pKa_2=10) : 3, 8, and 12. For alizarin red S (pKa_1=5.8 and pKa_2=10.8), the following pH were used: 2, 7 and 12 [40,41].

The UV-Vis spectra were measured directly after each preparation. It was done using an Ocean Optics Flame spectrometer (Model: FLMS00699) with a wavelength range from 300 to 850 nm. The integration time for each measurement ranged from 5 milliseconds to 10 milliseconds. The light source used was a Deuterium-Tungsten Halogen lamp covering the range of 300 nm to 850 nm. The blank was done using deionized water. This light source was coupled to the spectrometer using 400µm diameter optical fibers and positioned through a 1 cm quartz cuvette holder. The acquisition of spectra was facilitated by the Ocean View software.

NMR Spectrum

NMR spectra were acquired with a Bruker Advance Neo 500 spectrometer at the frequency of 500.07 MHz for ^1H and 125.76 MHz for ^{13}C equipped with a 5 mm double resonance broadband prodigy probe use nitrogen-cooled RF coils and preamplifiers. Chemical shifts were calibrated using the Tetramethysilane (0 ppm). For ^1H, we used a one 90° pulse with 64 scans and with a recycling time of 1s. For ^{13}C, we used a one 90° pulse with a ^1H decoupling waltz16 with 4096 scans and with a recycling time D1 of 2s. The ^1H and ^{13}C spectra were recorded in exactly the same conditions at room temperature and processed with a zero-filling factor of 2 and without an exponential decay. 5mg of either alizarin or alizarin red S were dissolved in 0.5mL of acetone-D_6. The ^1H and ^{13}C NMR spectra were also measured for alizarin red S in D_2O as it was more soluble than alizarin.

2.2. COMPUTATIONNAL METHOD

All calculations were carried out using the version 5.0.3 of the ORCA quantum chemistry program package and the version 6.5.1 of xTB [42,43].

Optimization Procedure

Ground and excited states properties were computed using density functional theory (DFT) and its time-dependent (TD-DFT) extension [44,45]. Optimized Geometries and Hessians were obtained using the PBE0 functional [46] complemented by the D3(BJ) dispersion correction [47,48]. Tight thresholds were employed for the self-consistent field (SCF) and optimization (tightSCF and tightopt keywords in ORCA nomenclature) [47,49]. The triple zeta def2-TZVP basis set, coupled with matching auxiliary basis sets, was consistently employed throughout all the computations [47,49,50]. All the optimized geometries can be found in the supplementary data 14.

Conformer and deprotonated Forms Search

Using Grimme's open-source Conformer-Rotamer Ensemble Sampling Tool (CREST), which relies on the xTB method, the exploration for deprotonated forms and conformer for the fully protonated form was conducted [43,51]. The geometries of the generated conformer or deprotonated forms were then subjected to optimization using the PBE0 functional. Finally, their single point energy (SPE) were obtained by using DLPNO-CCSD(T) computations with def2-TZVP basis sets with matching auxiliary basis sets and CPCM (water) [52]. Their SPE energies are then compared for each deprotonated or conformer forms to identify the most energetically stable forms (the one with the lowest SPE energy). By comparing the SPE energies, we can calculate the Boltzmann population distribution of each form. The identified stable forms correspond to the highest Boltzmann distribution. Those forms are dominant and are therefore selected for the following computations.

Solvation Models

Different solvation models were evaluated for UV-Vis and NMR spectra prediction. These models included the following:

-In vacuo: the molecule is studied in the absence of any solvent.

-Implicit solvation (water or acetone) using the linear response Conductor-like Polarizable Continuum Model (C-PCM) [53]. No solvents appear but it treats the solvent as a continuous medium surrounding the solute. This model accounts for the electrostatic and non-polar interactions between the solute and the solvent without explicitly representing individual solvent molecules. Their bulk properties are replaced by some macroscopic quantities (dielectric constant or solvent radius).

-A combined approach involving both implicit and explicit water molecules (either 1 water molecule per hydroxyl (OH) group or 3 water molecules per OH group). The water molecules were positioned to make hydrogen bonds with each hydroxyl group.

-Furthermore, a hybrid approach called Quantum Mechanics/Quantum Mechanics 2 (QM/QM2) [54–56] calculations were conducted by engaging between 70-100 water molecules It combines quantum mechanics (QM) for a region of interest (here the dye molecule) and the semi-empirical GFN2-xTB method [43,51] for the rest of the system (here the surrounding water molecules). The optimization was accomplished using the multiscale module in ORCA [42,57] together with the QM/QM2 ONIOM procedure. This allows detailed treatment for the electronic structure of the solute while considering the surrounding solvent at a less computationally expensive level. To consider the solvent effect, we also performed a Quantum Molecular Dynamics simulation of 25,000 steps with a 0.5 fs time step (other parameters selected as default such as a NHC (Nosé–Hoover chains) thermostat of 300K) [58]. An ellipsoid repulsive wall was added to keep the water molecules close to the substrate during the MS. From this simulation, 50 snapshots were selected, each 200 steps starting at 800. They were then optimized and the mean Vertical Energy (VE) of these snapshots calculated.

UV-Vis Spectrum computation

For Time-Dependent Density Functional Theory (TD-DFT) calculations concerning the UV-Vis spectrum, the B2PLYP functional was used with the resolution of identity method (RI) [30,59,60]. This choice is justified by previous theoretical benchmarks and preliminary calculations (see supplementary data 2) [61,62]. The UV-Vis VE calculations were done with the first 15 roots. The experimental spectra of the dyes studied (alizarin and alizarin red S) has only one band on the visible region. In all calculations, only the first excited state was considered for the VE calculation, as it can be compared to the experimental maximum absorption of the Visible region of the UV-Vis spectrum. The topology and form of the experimental spectra are due to vibrational and solvent effects which are not present when calculating the VE but will be accounted using another calculation. The color of the compound depends on the form of the spectra, it is therefore necessary to take it into account.

The vibrational contributions, including Herzberg–Teller effects [63–65], was accomplished using the Excited State Dynamics (ESD) module within ORCA [66]. Within this framework, the Adiabatic Hessian (AH) and Vertical Gradient (VG) approaches were used. As AH is a more complete and accurate method, computed spectra within the main text will be performed using this scheme [67]. VG spectra can be found in supplementary data 5. The AH calculations require the geometry of both Ground State (*GS)* and the first singlet excited state (S_1) geometries and frequencies, the VG ones only required the *GS* parameters, all of them computed at the DFT PBE0 level + CPCM. The VE energy and transition dipole moments were computed using the most accurate values *i.e.* RI-B2PLYP together with the appropriate solvation scheme (3 water molecules per OH). The linewidth was created using a Gaussian distribution and was fine-tuned to align with the Full Width at Half Maximum (FWHM) parameter of the experimental spectra, which depends on the concentration and other experimental parameters. To reduce the impact of experimental parameters like concentration, the computed and experimental spectra were normalized. This allows a direct comparison between the two spectra.

The CIELAB color coordinates was calculated for the UV-Vis spectra with an in-house script with illuminant D65 [68–70]. To quantify the quality of the color prediction, the color difference was quantified with ΔE_{2000} which is the latest ISO standard by CIE [71,72].

NMR Spectrum computation

Geometry optimization of tetramethylsilane (TMS), alizarin, alizarin red S molecules was conducted within vacuo, an implicit acetone or water solvent environment using the CPCM method or with explicit acetone or water molecules as described before. Subsequent computation of ^{1}H-NMR and ^{13}C-NMR shielding employed the revTPSS functional with D4 correction [73–75]. Basis set pcSseg-3 was selected for these calculations. Next, the isotropic shifts were used to compute the shifts that are comparable to the experimental by using this formula:

$$\sigma_{calculated} = \sigma_{TMS} - \sigma_{targetmolecule}$$

A summary of the computational protocol is summarized in a flow chart in the supplementary data 1.

2. RESULTS AND DISCUSSION

Fig.1 presents the structure of the studied molecules: alizarin (later referred as *H_2A*) and alizarin red S (later referred as *H_2ARS*). Both alizarin and alizarin red S have two acidic protons which can be subject to deprotonation depending on the solutions' pH. Alizarin (alizarin Red S) has pKa_1=5.5 and pKa_2=10 (pKa_1=5.8 and pKa_2=10.8) respectively. Therefore, in this study, we have chosen the following pH for each form: pH=3, pH=8, and pH=12 for alizarin and pH=2, pH=7 and pH=12 for alizarin red S [40,41].

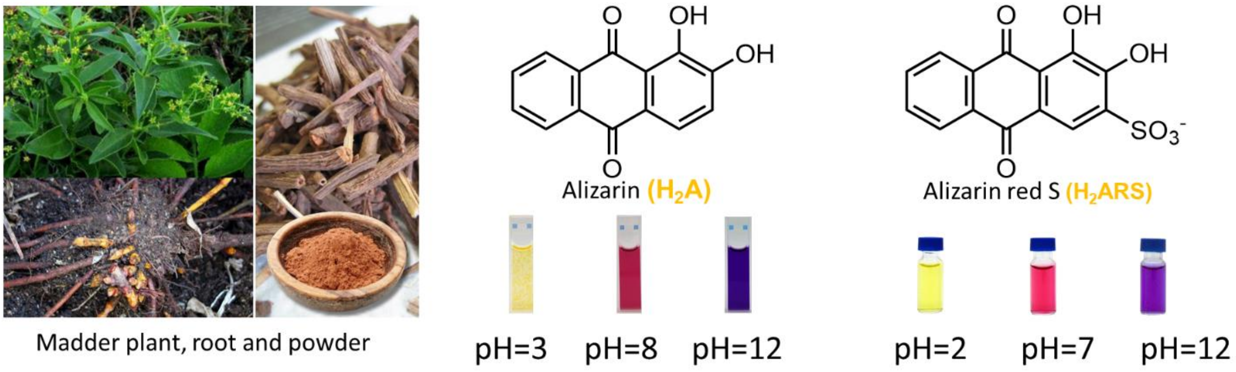

Fig. 1. (Left) Madder plant, its roots and powder. (Middle) Chemical structure of alizarin, abbreviated as H_2A and its alternative more soluble in water, alizarin red S (right), abbreviated as H_2ARS. The color of each molecule for different pH level are depicted below each structure.

This study aims to establish a reliable computational protocol in order to reproduce their spectroscopic properties (UV-Vis spectra, color and NMR spectra) and provide us with relevantchemical information.

3.1. ALIZARIN

3.1.1. UV-Vis spectra

3.1.1.1. *Conformer and deprotonated forms search*

The initial step involves exploring the conformer and deprotonated forms of alizarin for each pH range in order to identify the most stable forms.

In the protonated form (neutral) at pH=3, various studies have addressed the presence of different conformers [36,76]. We first generated the conformer of the neutral protonated form of alizarin and computed their Single Point Energy (SPE). The one with the lowest SPE energy after optimization is the most stable and is taken as a reference. The other conformer forms are listed by energy (in kcal/mol) with respect to the most stable form in Fig 2. We have found that the dominant form is the one with the hydrogen of both the α and β-hydroxyl groups making hydrogen bonds with the neighboring oxygen. It will be later referred to as H_2A. Furthermore, for the ground state, the forms with the proton transfer on the ketone as reported in previous publications are much higher in energy (14.07 kcal/mol respective to H_2A), meaning that in the ground state, there is likely no proton transfer for the neutral form in water. The remaining conformer forms do not exist in solution as they are higher in energy than the most stable one.

For the mono-deprotonated form (monoanionic) at pH=8, two potential forms are possible due to the presence of two deprotonation sites (see Fig. 2). However, by comparing the computed SPE, the most stable configuration is the one with the β-hydroxyl being deprotonated. The other form with the α hydroxyl deprotonated is higher in energy by 0.9 kcal/mol. This corresponds to the Boltzmann distribution of 82% in favor of the most stable form. This can be explained by the formation of intramolecular hydrogen bonds between the ketone and the α hydroxyl group, making it more stable and therefore less favorable to deprotonation than the β-hydroxyl group. Furthermore, the hydrogen in the β position can be more accessible to the surrounding solvent, making it more susceptible to deprotonation. The most stable form will be used to do further calculations as it will be the most dominant. We will denote it as HA^-.

For the di-deprotonated (dianionic) form at pH=12, there is only one stable form without other conformers. It will be denoted as A^{2-}.

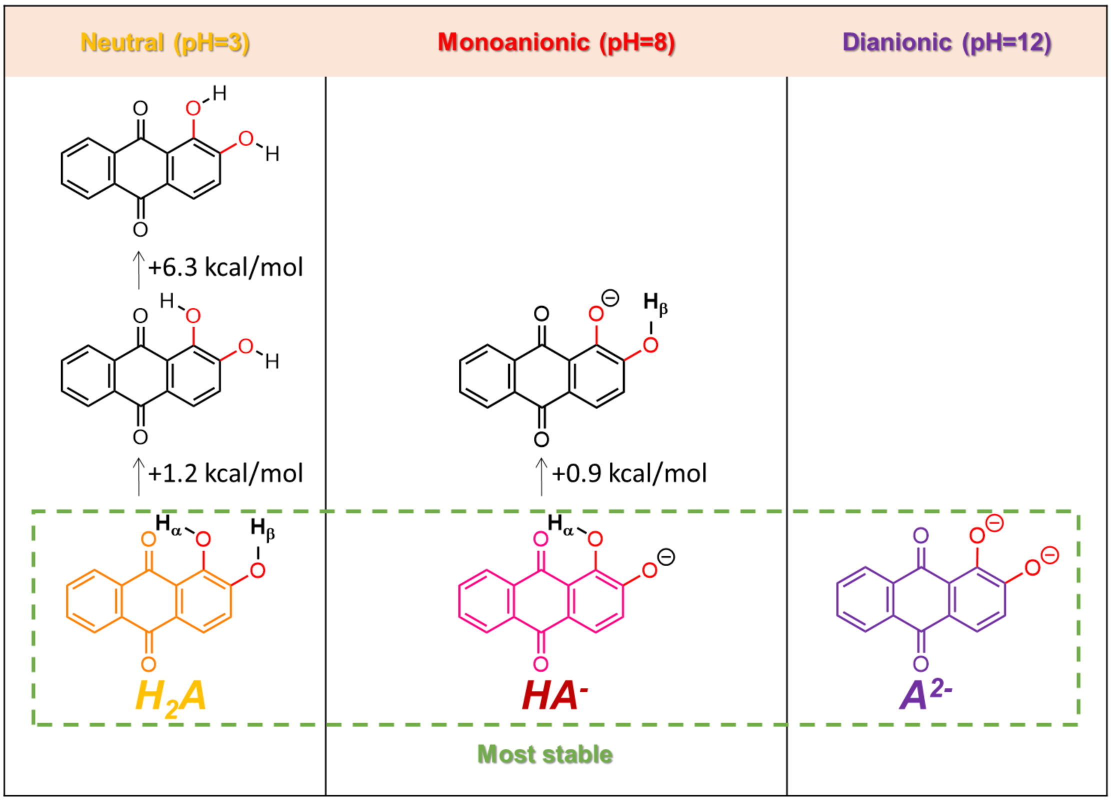

Fig. 2. Alizarin rotamers and deprotonated forms for each pH range and their relative energies. For the fully protonated form at pH=3. The geometries are sorted from the most stable form to the less stable form. The most stable forms are denoted H_2A (neutral form), HA^- (monoanionic form), and A^{2-} (dianionic form).

3.1.1.2. Vertical energy and choice of solvation model

In computational chemistry, the choice of solvation model is critical as it determines the accuracy of the predicted UV-Vis spectra [77]. In fact, the geometry of the molecules can be influenced by the surrounding solvent via specific interactions like hydrogen bonds, ion pairs, π-interactions, etc. Here, we have tested different solvation models to compute the VE between the electronic *GS* and S_1 and compare it to the maximum absorption of the experimental visible spectra. The calculations were first done in vacuo, then with implicit water, a combined implicit and explicit, and finally with a multi-level approach such as QM/QM2 in combination with Molecular Dynamics. All computational details of those solvation models are outlined in the *Methods* section. Fig.3 presents a condensed view of the different models used in this study and the associated results for the alizarin forms H_2A, HA^- and A^{2-} *(Additional information can be found in supplementary data 3*).

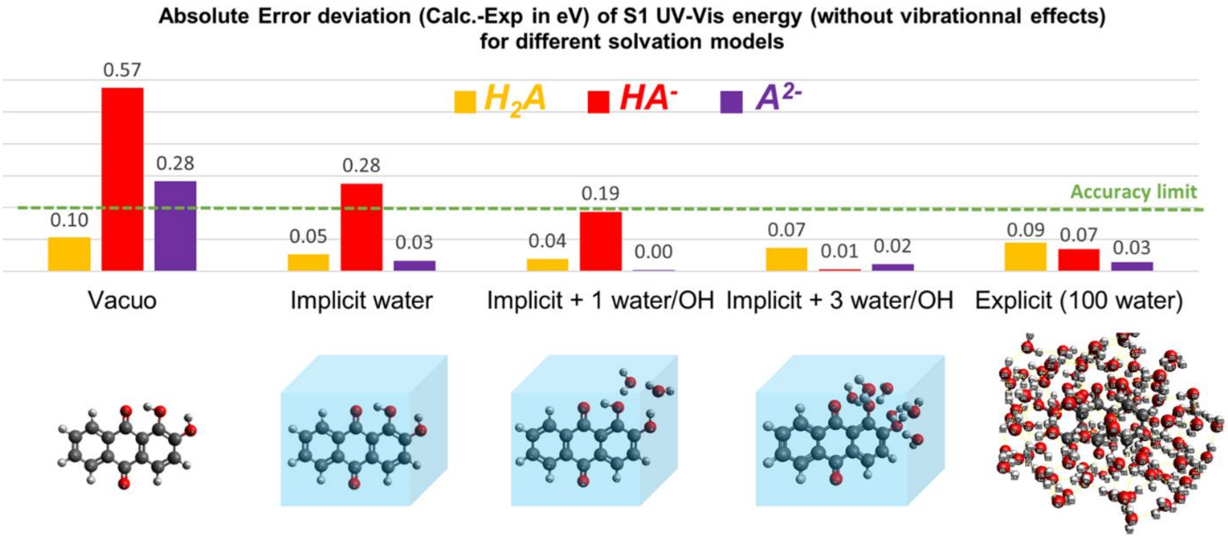

Fig. 3. (Top) Absolute energy difference between the calculated VE and the experimental absorption energy for the different solvation models of alizarin. The yellow stands for the H_2A form, the red for HA^- one and the purple for A^{2-}. The accuracy threshold is fixed at 0.2 eV according to the literature. (Bottom) Different solvation models were used. From left to right: alizarin in vacuo, implicit water, implicit with 1 water per hydroxy group, implicit with 3 water per hydroxy group, QM/QM2 with 100 explicit water (over 50 snapshots).

We first did the calculations in vacuo, without any solvent as a study case. However, it does not provide insights into the effects of a surrounding medium, which is often crucial for realistic scenarios. Here, it was observed that for the neutral form, the vacuo model is accurate enough (the error deviation falls below the 0.2eV accuracy limit which is the standard in the literature). However, for the deprotonated forms (monoanionic HA^- or dianionic A^{2-}), the vacuo model is not accurate enough (error deviation of 0.57eV for AH^- and 0.28eV for A^{2-}). It is therefore necessary to include solvent effects for these forms.
A first approximation of the solvent effect can be done by using an implicit model. For alizarin, implicit solvation gives better agreement with experimental data by reducing the error by at least half (it falls to 0.05eV for H_2A, 0.28eV for HA^- and 0.03eV for A^{2-}). It can be used to test different solvent environments while being computationally efficient. This approach is useful for the case where there is no apparent interaction between the solvent and the dye, like the neutral form H_2A in water or for apolar solvents. However, the HA^- form is still above the accuracy limit (with 0.28 eV error deviation) in implicit calculation. Therefore, we need to account for specific solvent effects. For those forms, the model can be refined by adding some explicit solvent molecules near the hydroxyl sites. Explicit water molecules (either 1 or 3) per hydroxy group were tested. This considerably reduces the calculated and experimental energy difference for the deprotonated forms. Among them, the best model is the one with 3 explicit water molecules near the OH sites (error deviation of 0.01 eV for HA^- and 0.02 eV for A^{2-}). This shows that for the deprotonated forms, solvent interactions like hydrogen bonds are mandatory to accurately model the absorption energy. Therefore, this combined model can be a good compromise to accurately predict the UV-Vis energies for a low computational cost. It can be used when there is a specific solute-solvent interaction.

Finally, the last model tested was QM/QM2 with 100 explicit water which represents a theoretical best estimate for our protocol. For each form, a quantum molecular dynamic was performed followed by computing the VE of 50 snapshots. Here, it was observed that across all the forms, the QM/QM2 results consistently fall below the 0.2 eV accuracy threshold (0.09 eV for H_2A, 0.07 eV for HA^- and 0.03 eV for A^{2-}). This implies that QM/QM2 is a reliable method for predicting the properties of new molecules for which the solute-solvent interactions are predominant but requires a much higher computational cost, at least 50 times higher. More information about the MD and the selected snapshots can be found in supplementary data 4.

From the previous paragraphs, it is clear that the accuracy of the VE is tightly bound to how the environmental effects are modeled. As water is a highly polar solvent and involved in multiple inter-molecular interactions, one should expect that explicit molecules have to be added. Interestingly, for some forms, implicit solvation is accurate enough, notably for A^{2-}, where two charged oxygens are present. However, only the microsolvation with 3 added water molecules per OH is sufficient to get close to the experimental measurements for all forms. This model also gives similar results in comparison to a full explicit model, allowing us to ensure that it is reliable and transferable to similar dyes.

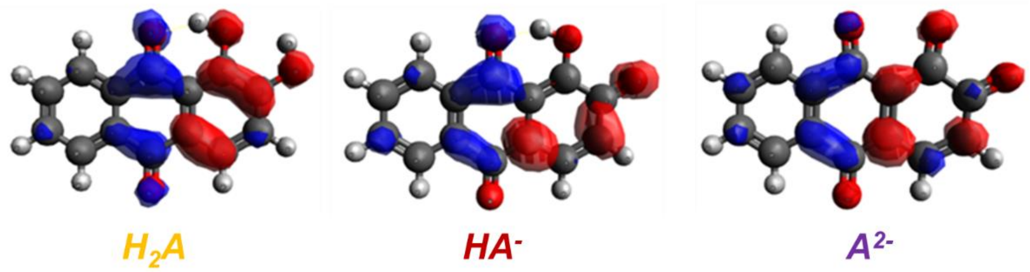

Fig. 4. Difference in electronic densities for the GS-> S_1 transition for alizarin for different protonation states. The blue orbital represents a decrease in electronic density. The red one represents an increase in electronic density. The isovalue is 0.02 a.u.

To further delve into the nature of electronic transitions, the difference in electronic densities has been calculated for the transition $GS \rightarrow S_1$ (which corresponds to the absorption in the visible part of the UV-Vis spectrum). The result for each alizarin form is depicted in Fig.4.

For the neutral form H_2A, the transition involves a combined n->π (owing to the presence of oxygen) and π-> π* transition, with a more pronounced π-> π*character. As we progress to the deprotonated form, HA^- and A^{2-}, the transition nature shifts more towards π-> π* transition rather than n->π* as the deprotonated hydroxy groups become part of the conjugated system.

3.1.1.3. Computed absorption spectra and CIELAB color

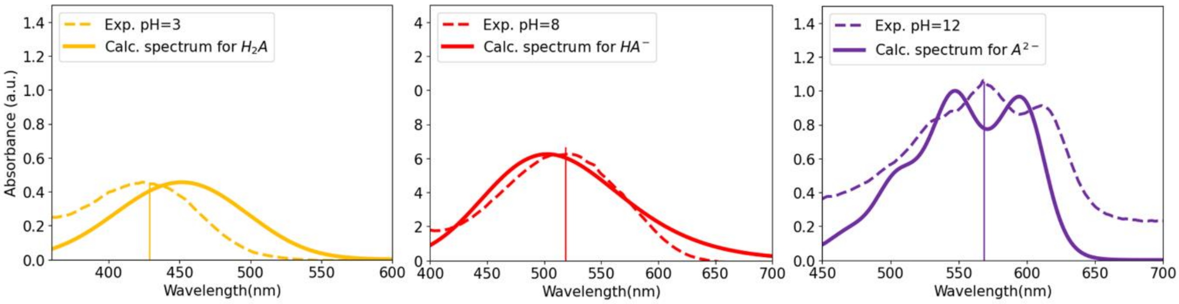

	Experimental (normalized)				Calculated (normalized)				ΔE_{2000}
Form	L*	a*	b*	color	L*	a*	b*	color	
H_2A	99.0	-13.4	68.4	🟨	90.7	6.9	80.4	🟨	**13.3**
HA^-	67.5	53.3	0.9	🟥	59.1	45.5	3.2	🟥	**7.5**
A^{2-}	54.1	51.9	-50.0	🟪	57.0	61.7	-53.6	🟪	**4.1**

Fig. 5. (Top) The calculated and experimental UV-Vis spectra for alizarin at different pH. The dotted line is the experimental one. The

full lines are the calculated spectrum with the Adiabatic Hessian (AH) method. The vertical lines correspond to the computed VE. (Bottom) Predicted and computed colors of different alizarin forms with CIELAB coordinates (L, a*, b*) and the calculated color variation between computed and experimental color coordinates with* ΔE_{2000}.

The VE alone is not enough to predict the full spectrum because it does not consider vibrational effects which can be responsible for the UV-Vis spectra topology (shape). In Fig.5. we have computed the absorption spectrum of alizarin at different pH and compared them with their experimental UV-Vis spectra. First, if we look at the different pH forms of alizarin we can see that their UV-Vis spectra shape and color differ. When the pH increases, we see a red shift of the spectra together with a hyperchromic shift (increase in absorption intensity). For pH=3, the spectrum has a maximum absorption peak at 430nm, resulting in a yellow solution. For pH=8, the solution turns red, with the maximum absorption at 530 nm. For pH=12, the solution takes a violet hue, with a maximum peak at 570 nm and two shoulders at 530 nm and 610 nm. These additional features could be attributed to several electronic transitions or a combination of electronic and vibrational effects. To discern the nature of each transition, we used the Adiabatic Hessian method (AH). The details of the computation can be found in the *Methods* section.

Overall, the computed spectra with AH are in good agreement with experimental data for both the maximum and topology, in particular for HA^- and A^{2-}. For H_2A, the computed spectrum is shifted by about (27 nm) but it can be explained by the low solubility of the neutral form in water, preventing us from having a reliable UV-Vis spectrum.
The A^{2-} replicates the experimental topology with three distinct shoulders. The VE corresponds to one electronic transition from $GS \rightarrow S_1$. The middle peak is therefore attributed to one electronic transition, while the shoulders around 540 nm and 610 nm result from vibronic effects.

While the absorption spectra are really useful in spectroscopic studies, in the cultural heritage or dyeing field, the color of the molecule is the key property. In order to gain access to this information we can convert the UV-Vis spectra to color CIELAB coordinates. CIELAB color space is a color model introduced by the Commission Internationale de l'Eclairage (International Commission on Illumination or CIE) to provide a uniform and consistent representation of colors [69]. It is designed to be independent of devices and illuminants, making it useful for comparing colors across different conditions. Here, we will use it to compare the computed and experimental color. The colors are expressed in L*a*b* coordinates. L stands for Lightness and corresponds to the perceived brightness of the color. The values range from 0 (black) to 100 (white). The a* stands for the position on the red(positive) to green (negative). b* stands for blue (negative) to yellow (positive). The CIELAB color space is represented in supplementary data 6. The bottom part of Fig.5 illustrates the predicted and experimental along with their respective CIELAB coordinates. ΔE_{2000} is the latest standard created by the CIE and quantifies the color difference. E stands for "Empfindung" which is the German word for sensation and 2000 stands for the version of standard (older versions exist like ΔE_{76} or ΔE_{94}) [68,71]. The standard perception ranges as follows:

- <= 1.0: Not perceptible by the human eye
- 1-2: Perceptible through close observation
- 2-10: Perceptible at a glance
- 11-49: Colors are more similar than the opposite
- 100: Colors are exactly the opposite

The computed color closely resembles the experimental ones. A higher ΔE_{2000}=13.3 is observed for the H_2A form and HA^- (ΔE_{2000}=7.57), possibly attributed to the lower solubility of alizarin in water, where a non-negligible precipitate can be observed. In contrast, for A^{2-} which is more soluble in water, its computed color is similar to the experimental (ΔE_{2000}=4.1). That means that the color is similar but the difference can be perceptible to the human eye at a glance. While the CIELAB colors are predominantly used for non-liquid systems, our approach shows that computations can be modeled with a reasonably good accuracy.

3.1.2. NMR shift prediction

Another key property of chemical systems is their NMR spectra. It is often used to decipher the structure of molecules in a complex environment, like pigments used in paintings, which are composed of a dye complexed with a metallic cation. Our protocol will aim at reproducing with good accuracy the experimental peaks.

Here, we present a study case with alizarin. The computed ^{1}H shift values were compared to the experimental spectra of alizarin in acetone-D_6 (chosen because alizarin is not soluble in water) in Table 1. We tested the influence of the solvation model with implicit and 3 explicit acetones following the UV spectrum protocol. The calculated ^{1}H NMR shift differs by less than 0.16 ppm on average with respect to the experimental one for aromatic hydrogens in implicit acetone and 0.22 ppm on average for explicit and implicit acetone. This suggests a good level of accuracy for the prediction of proton chemical shifts for both solvation models. The prediction of the ^{1}H shifts for hydrogens H3, H4, H6, and H7 are better with implicit than explicit. However, it is noted that the accuracy is worse when dealing with the labile hydrogens in the hydroxy (-OH) group (H1 and H2) with implicit solvation. Labile hydrogen is prone to exchange with the surrounding solvents, it is therefore necessary to add explicit acetones near the hydroxy groups. For labile hydrogens, the explicit solvation model yields better accuracy. Furthermore, H5-H8 are better with explicit than implicit models. Explicit solvation is therefore more suited for labile hydrogens. The experimental spectra are depicted in supplementary data 7, along with its attribution, which was done by confronting the computed shifts.

Table 1. Computed and experimental ^{1}H chemical shift of alizarin in acetone-D_6 with the respective error deviation in ppm or % for implicit or implicit and explicit solvation model.

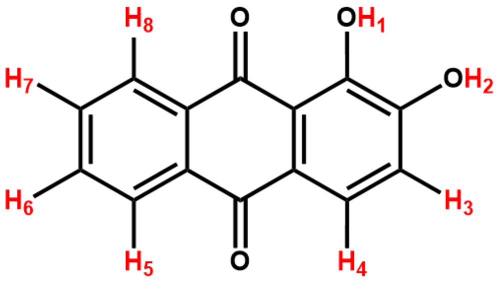

	Exp. (ppm)	Calc. (ppm)		Calc.-error (ppm)		Calc.-error (%)	
Attribution	**In acetone-D_6**	**Implicit**	**Explicit**	**Implicit**	**Explicit**	**Implicit**	**Explicit**
1	12.8	15.1	11.5	2.3	-1.3	18.2	10.2
2	9.3	7.2	10.0	-2.1	0.6	22.5	7.0
3	7.3	7.4	7.6	0.1	0.2	1.3	3.4
4	7.8	8.0	8.2	0.2	0.4	3.0	5.4
5	8.3	8.5	8.5	0.2	0.1	2.2	1.6
6	8.0	8.1	8.1	0.1	0.1	1.6	1.9
7	8.0	8.0	8.2	0.1	0.2	1.0	2.7
8	8.3	8.5	8.4	0.3	0.1	3.0	1.5

3.1.3. Experimental uncertainty due to solubility

As raised multiple times in this part, alizarin has a poor solubility in water. The color of alizarin in solution is highly sensitive to experimental conditions such as concentration, pH and temperature. The maximum absorption remains constant but the shape can potentially alter. Consequently, the measured color may vary and a higher delta E can be calculated with respective to the computed color. To address this experimental obstacle, we opted for its alternative, alizarin red S which exhibits greater solubility.

3.2. ALIZARIN RED S

As we have seen, the limited solubility of alizarin in water can pose challenges when measuring their experimental UV-Vis and NMR spectra due to the potential formation of precipitates. To address this concern, a more soluble analogue, alizarin red S, has been studied.

3.2.1. Conformer and deprotonated forms search

For the acidic form (pH=2) of alizarin red S, different conformer forms can exist. We computed the energies of the possible conformer and sorted them in Fig. 6. Like alizarin, we do not observe any proton transfer for the ground state. The most stable form shows a hydrogen on the α position pointing towards the ketone, making a hydrogen bond, while the β-hydrogen is pointing on the opposite side towards the negatively charged sulfonic group. It will be noted as H_2ARS. The other conformer forms do not exist as they are much higher in energy (hence low Boltzmann distribution).

For the mono-deprotonated form (pH=7), two possible forms can exist (see Fig.6). The comparison between energies point out that the β-hydroxyl deprotonated is the most stable configuration, the α-hydroxyl making a hydrogen bond with the ketone and is less susceptible to deprotonation. This form will be noted as *$HARS^-$*. For the di-deprotonated form (pH=12), there is only one form that will be denoted as *ARS^{2-}*.

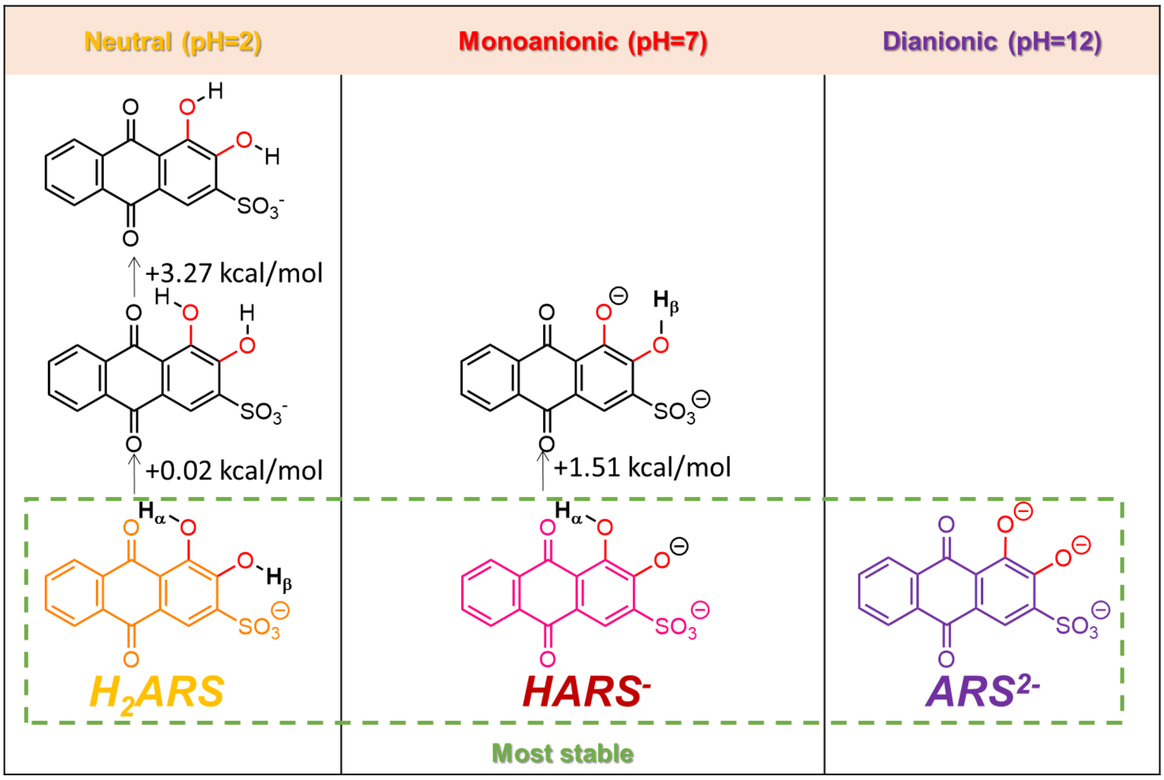

Fig. 6. Alizarin red S rotamer and deprotonated for each pH range, along with their relative energies. For the acidic form, the other forms are much higher in energy (>17 kcal/mol) and are not considered. The most stable forms are denoted H_2ARS (acidic form), $HARS^-$ (mono-deprotonated form), and ARS^{2-} (di-deprotonated form).

3.2.2. UV-Vis spectra prediction

The experimental spectra have maximum absorption energy at 425nm for *H_2ARS*, 521nm for *$HARS^-$* and 560 nm for *ARS^{2-}* with two shoulders at 600nm and 530nm. The computed spectra were done considering the method and protocol used for alizarin. The results are depicted in Fig.7. There is a better agreement between the experimental and computed spectra for the *H_2ARS and $HARS^-$* form than alizarin, which can be explained by a higher solubility of alizarin red S. The computed VE matches perfectly the experimental one. Similarly, the AH spectra of the *$HARS^-$* and *ARS^{2-}* are in adequation with the experimental ones, in both the topology and position of the spectra.

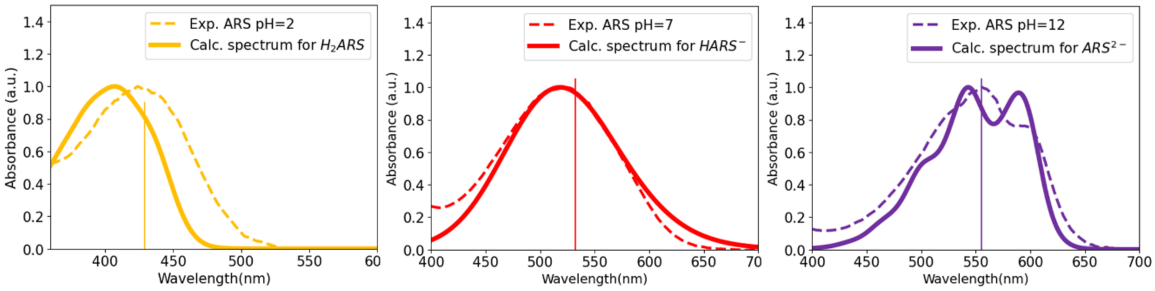

	Experimental (normalized)				Calculated (normalized)				ΔE_{2000}
Form	L*	a*	b*	color	L*	a*	b*	color	
H_2ARS	99.6	-10.8	77.3	🟨	99.2	-14.0	68.0	🟨	**3.3**
$HARS^-$	65.4	54.8	-3.2	🟥	59.1	57.7	-17.8	🟥	**8.3**
ARS^{2-}	54.4	51.0	-50.9	🟪	57.0	61.7	-53.6	🟪	**4.0**

Fig. 7. (Top) The calculated and experimental UV-Vis spectra for alizarin red S at different pH. The dotted line is the experimental one. The full lines are the calculated spectrum with Adiabatic Hessian (AH) method. The vertical lines correspond to the computed VE. (Bottom) Predicted and computed colors of different alizarin red S forms with CIELAB coordinates (L, a*, b*) and the calculated color variation between computed and experimental color coordinates with ΔE_{2000}.*

To assess the quality of the color prediction, the calculated and experimental color CIELAB are represented in Fig.7. The calculated color matches the observed experimental color, with higher accuracy for the H_2ARS form (3.31 for alizarin red S and 13.32 for alizarin, see Fig.5). This can be explained again by its higher solubility compared to alizarin.

The additional sulfonic group does not change the color of the compound compared to alizarin. This can be explained by the difference densities plotted in Fig.8. The sulfonic group does not participate in the electron delocalization for the $GS \rightarrow S_1$ transition.

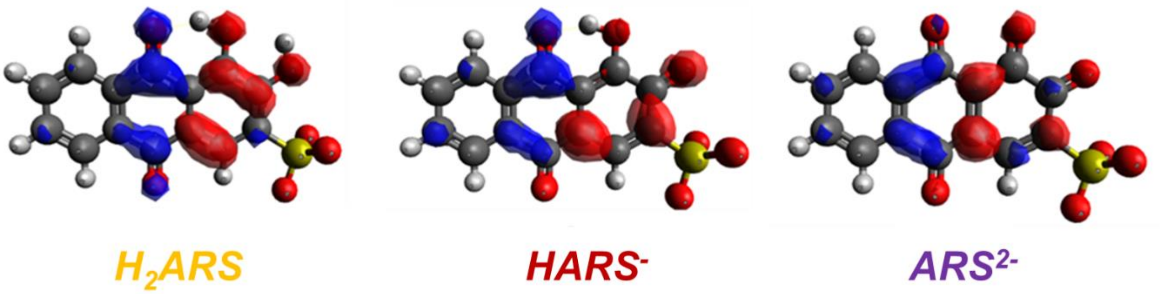

Fig. 8. Difference electronic densities for the GS-> S_1 transition for alizarin red S for different protonation states. The blue orbital represents a decrease in electronic density. The red one represents an increase in electronic density. The isovalue is 0.02 a.u.

3.2.3. ^{1}H and ^{13}C NMR prediction

Thanks to the higher solubility of alizarin red S in water, the measure of NMR spectra in D_2O is possible. We have obtained the ^{1}H NMR spectra of H_2ARS in acetone-D_6 only as the one in water gives very broadened signals, probably due to exchange processes at room temperature which is consistent with other publications [26]. Following the best computational protocol for alizarin, the calculations were done using an explicit solvation scheme. All the geometries are accessible in the supplementary data 14. The comparison between the computed ^{1}H chemical shifts is represented in Table 2 (in acetone-D_6) and ^{13}C in Table 3 (for both acetone-D_6 and D_2O). The error deviation of aromatic hydrogens (H3 to H7) is less than 0.2 ppm in average (which represents 2.1% in mean error deviation). This error is less than for alizarin (which has 2.8% mean error deviation). There is a better agreement with experimental data for alizarin red S, again explained by its higher solubility compared to alizarin. The labile hydrogens are less accurate with 17% of error deviation for H2 and 11% for H2. The experimental and computed shifts can be found for different alizarin red S forms in supplementary data 8 to 13.

Table 2. Computed and experimental chemical shift of alizarin red S in acetone-D_6 with the respective error deviation in ppm or %.

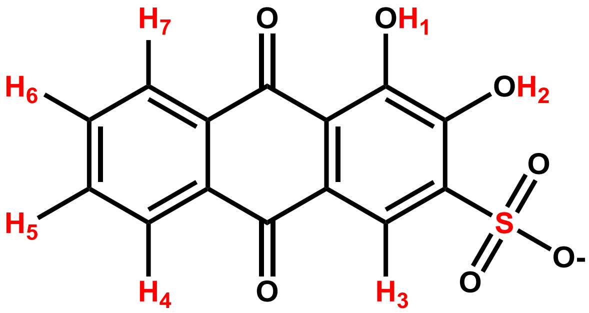

Attribution	Exp. (ppm) in acetone-D_6	Calc. (ppm)	Calc.-error (ppm)	Error deviation (%)
H1	12.8	15.0	2.2	17.1
H2	11.9	13.2	1.3	11.1
H3	8.2	8.4	0.2	2.7
H4	8.3	8.5	0.2	2.7
H6-H5	7.9	8.0	0.1	1.3
H6-H5	7.9	8.0	0.1	1.3
H7	8.3	8.5	0.2	2.5

The comparison between the computed and experimental ^{13}C shifts in D_2O for alizarin red S is represented in Table 3. It shows that the error deviation of Carbons C4-C14 are less than 6 ppm on average (which represents 4.4 % in mean error deviation). There is a higher error deviation for carbons that are next to a hydroxy or sulfonic group (C1-C3) with up to 5.5% error deviation.

Overall, there is a good agreement between the computed and experimental chemical shifts for both ^{1}H and ^{13}C NMR spectra. This protocol proves to be efficient in predicting NMR spectra.

Table 3. Computed and experimental chemical ^{13}C shift of alizarin red S in acetone-D_6 or D_2O with the respective error deviation in ppm or %.

	Acetone-D_6		**D_2O**	
Attribution	Calc.-error (ppm)	Error deviation (%)	Calc.-error (ppm)	Error deviation (%)
1	8.2	5.5	9.8	6.5
2	7.9	5.2	8.6	5.7
3	6.7	5.0	4.7	3.5
4	5.0	4.2	3.9	3.3
5	4.0	3.3	5.5	4.5
6	6.9	3.8	6.7	3.7
7	4.2	3.1	6.5	4.9
8	4.4	3.4	4.7	3.7
9	3.5	2.5	5.2	3.9
10	3.4	2.5	6.2	4.7
11	3.9	3.1	4.4	3.5
12	4.4	3.3	6.7	5.1
13	5.3	2.8	7.0	3.7
14	4.3	3.7	4.8	4.1

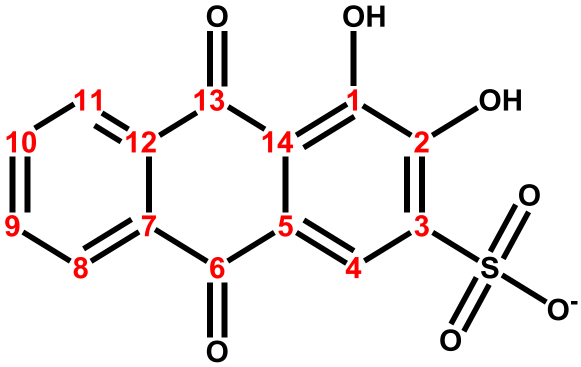

4. CONCLUSION

Deciphering experimental spectra of natural dyes is a persistent challenge due to the presence of impurities, extraction difficulties, solubility issues, fast degradation, and so on. In this context, computational spectroscopy appears as a solution for the elucidation of complex structures of pigments. Here, we focus on Madder, a natural dye with historical importance. By combining computational insights with experimental data, our study has demonstrated the great efficiency of the optimized computational protocol for accurately predicting UV-Vis spectra, CIELAB color coordinates, and NMR shift of alizarin, the main coloring molecule of Madder, and its analog alizarin red S. In particular, we have found that the incorporation of conformer, deprotonated forms for each pH, solvation models, and careful consideration of solvent interactions resulted in accurate description when compared with experimental measurements. The computed spectra closely match the experimental data, providing a reliable foundation for the prediction of other hydroxyanthraquinones and numerous colored dyes. The computation of CIELAB coordinates of these 2 molecules also yields good results despite some issues due to solubility. This approach can be of interest to extracting the contribution of each dye in a mixture or for predicting new hues of colored molecules. By overcoming experimental complexities, this protocol accelerates the development of compounds tailored to specific needs by predicting with accuracy several properties. This optimized computational protocol outlined here offers a versatile tool for designing novel molecules across a wide variety of coloring industries, such as textiles, cosmetics, food, pharmaceuticals, and art. Furthermore, it can set the stage for deeper exploration into more complex structures of pigments, which are often challenging to elucidate by experimental methods.

▪AUTHOR INFORMATION

Linh Thanh Huyen TRAN: linh.tran@sorbonne-universite.fr

Baptiste RIGAUD: baptiste.rigaud@sorbonne-universite.fr

Maguy JABER: maguy.jaber@sorbonne-universite.fr

Romain BERRAUD-PACHE: romain.berraud-pache@sorbonne-universite.fr

▪REFERENCES

[1] Baroni A, Comite V, Guglielmi V, Casanova M, Redegalli P, Fermo P. Identification of natural dyes in historical tapestries, a LC-MS/MS approach. J Phys: Conf Ser 2022;2204:012065. https://doi.org/10.1088/1742-6596/2204/1/012065.

[2] Casadio F, Leona M, Lombardi JR, Van Duyne R. Identification of Organic Colorants in Fibers, Paints, and Glazes by Surface Enhanced Raman Spectroscopy. Acc Chem Res 2010;43:782–91. https://doi.org/10.1021/ar100019q.

[3] Fonseca B, Schmidt Patterson C, Ganio M, MacLennan D, Trentelman K. Seeing red: towards an improved protocol for the identification of madder- and cochineal-based pigments by fiber optics reflectance spectroscopy (FORS). Herit Sci 2019;7:92. https://doi.org/10.1186/s40494-019-0335-1.

[4] Brommelle N. Material for a History of Conservation. The 1850 and 1853 Reports on the National Gallery. Studies in Conservation 1956;2:176. https://doi.org/10.2307/1504963.

[5] De Viguerie L, Michelin A, Radepont M, Pottier F, Alfeld M, Walter P, et al. Imagerie hyperspectrale pour l’analyse d’œuvres peintes. In: Benech C, Cantin N, Languille M-A, Mazuy A, Robinet L, Zazzo A, editors. Instrumentation portable, Editions des archives contemporaines; 2019, p. 43–65. https://doi.org/10.17184/eac.2457.

[6] Pronti L, Mazzitelli J-B, Bracciale MP, Massini Rosati L, Vieillescazes C, Santarelli ML, et al. Multi-technique characterisation of commercial alizarin-based lakes. Spectrochimica Acta Part A: Molecular and Biomolecular Spectroscopy 2018;200:10–9. https://doi.org/10.1016/j.saa.2018.04.008.

[7] Silva LC, Otero V, Melo MJ, Cabrita EJ, Mafra L. What’s the Madder? Characterization of Old Fashioned Alizarin/Aluminum Red Pigments Using Liquid and Solid-State NMR. Colorants 2023;2:601–17. https://doi.org/10.3390/colorants2040031.

[8] Blackburn RS. Natural dyes in madder (*Rubia* spp.) and their extraction and analysis in historical textiles. Coloration Technol 2017;133:449–62. https://doi.org/10.1111/cote.12308.

[9] Janssens K, Van Der Snickt G, Vanmeert F, Legrand S, Nuyts G, Alfeld M, et al. Non-Invasive and Non-Destructive Examination of Artistic Pigments, Paints, and Paintings by Means of X-Ray Methods. Top Curr Chem (Z) 2016;374:81. https://doi.org/10.1007/s41061-016-0079-2.

[10] Creagh DC. The characterization of artefacts of cultural heritage significance using physical techniques. Radiation Physics and Chemistry 2005;74:426–42. https://doi.org/10.1016/j.radphyschem.2005.08.011.

[11] Krizsán K, Szókán Gy, Toth ZA, Hollósy F, László M, Khlafulla A. HPLC Analysis of Anthraquinone Derivatives in Madder Root (Rubia Tinctorum) and Its Cell Cultures. Journal of Liquid Chromatography & Related Technologies 1996;19:2295–314. https://doi.org/10.1080/10826079608017158.

[12] Degano I, Tognotti P, Kunzelman D, Modugno F. HPLC-DAD and HPLC-ESI-Q-ToF characterisation of early 20th century lake and organic pigments from Lefranc archives. Herit Sci 2017;5:7. https://doi.org/10.1186/s40494-017-0120-y.

[13] Rafaelly L, Heron S, Nowik W, Tchapla A. Optimisation of ESI-MS detection for the HPLC of anthraquinone dyes. Dyes and Pigments 2008;77:191–203. https://doi.org/10.1016/j.dyepig.2007.05.007.

[14] Cosentino A. FORS Spectral Database of Historical Pigments in Different Binders. E-Cons 2014:54–65. https://doi.org/10.18236/econs2.201410.

[15] Cruz Mojica K, León Santiago M, Varela García E, Reyes Lezama M, Tapia Mendoza E. New progress in the extraction and identification of Mexican cochineal (Dactylopius coccus) in fresh dyed wool and dyed wool with artificially accelerated aging and color description. Color Research & Application 2023;48:151–64. https://doi.org/10.1002/col.22828.

[16] Baroni A, Comite V, Guglielmi V, Casanova M, Redegalli P, Fermo P. Identification of natural dyes in historical tapestries, a LC-MS/MS approach. J Phys: Conf Ser 2022;2204:012065. https://doi.org/10.1088/1742-6596/2204/1/012065.

[17] Whitney AV, Casadio F, Van Duyne RP. Identification and Characterization of Artists' Red Dyes and Their Mixtures by Surface-Enhanced Raman Spectroscopy. Appl Spectrosc 2007;61:994–1000. https://doi.org/10.1366/000370207781745838.

[18] Ford L, Rayner CM, Blackburn RS. Degradation of lucidin: New insights into the fate of this natural pigment present in Dyer's madder (Rubia tinctorum L.) during the extraction of textile artefacts. Dyes and Pigments 2018;154:290–5. https://doi.org/10.1016/j.dyepig.2018.03.023.

[19] Ford L, Henderson RL, Rayner CM, Blackburn RS. Mild extraction methods using aqueous glucose solution for the analysis of natural dyes in textile artefacts dyed with Dyer's madder (Rubia tinctorum L.). Journal of Chromatography A 2017;1487:36–46. https://doi.org/10.1016/j.chroma.2017.01.053.

[20] Barone V, Alessandrini S, Biczysko M, Cheeseman JR, Clary DC, McCoy AB, et al. Computational molecular spectroscopy. Nat Rev Methods Primers 2021;1:38. https://doi.org/10.1038/s43586-021-00034-1.

[21] Chenciner R. Madder Red: A History of Luxury and Trade. Routledge; 2003.

[22] Tian G, Cui R, Liu C, Hu X. Natural Dyeing with Madder: Exploring Traditional Techniques and Color Characteristics. Fibres & Textiles in Eastern Europe 2023;31:10–21. https://doi.org/10.2478/ftee-2023-0031.

[23] Hui-Yu J. Studies on the photofading of alizarin, the main component of madder | Elsevier Enhanced Reader 2020. https://doi.org/10.1016/j.dyepig.2020.108940.

[24] Ackacha MA, Połeć-Pawlak K, Jarosz M. Identification of anthraquinone coloring matters in natural red dyestuffs by high performance liquid chromatography with ultraviolet and electrospray mass spectrometric detection. Journal of Separation Science 2003;26:1028–34. https://doi.org/10.1002/jssc.200301484.

[25] Cuoco G, Mathe C, Archier P, Vieillescazes C. Characterization of madder and garancine in historic French red materials by liquid chromatography-photodiode array detection. Journal of Cultural Heritage 2011;12:98–104. https://doi.org/10.1016/j.culher.2010.05.005.

[26] Justino LLG, Braz S, Ramos ML. Spectroscopic and DFT Study of Alizarin Red S Complexes of Ga(III) in Semi-Aqueous Solution. Photochem 2023;3:61–81. https://doi.org/10.3390/photochem3010005.

[27] Amat A, Miliani C, Romani A, Fantacci S. DFT/TDDFT investigation on the UV-vis absorption and fluorescence properties of alizarin dye. Phys Chem Chem Phys 2015;17:6374–82. https://doi.org/10.1039/C4CP04728A.

[28] Mech J, Grela MA, Szaciłowski K. Ground and excited state properties of alizarin and its isomers. Dyes and Pigments 2014;103:202–13. https://doi.org/10.1016/j.dyepig.2013.12.009.

[29] Cysewski P, Jeliński T, Przybyłek M, Shyichuk A. Color prediction from first principle quantum chemistry computations: a case of alizarin dissolved in methanol. New J Chem 2012;36:1836. https://doi.org/10.1039/c2nj40327g.

[30] Jacquemin D, Brémond E, Planchat A, Ciofini I, Adamo C. TD-DFT Vibronic Couplings in Anthraquinones: From Basis Set and Functional Benchmarks to Applications for Industrial Dyes. J Chem Theory Comput 2011;7:1882–92. https://doi.org/10.1021/ct200259k.

[31] Anouar EH, Osman CP, Weber J-FF, Ismail NH. UV/Visible spectra of a series of natural and synthesised anthraquinones: experimental and quantum chemical approaches. SpringerPlus 2014;3:233. https://doi.org/10.1186/2193-1801-3-233.

[32] Berenbeim JA, Boldissar S, Owens S, Haggmark MR, Gate G, Siouri FM, et al. Excited state intramolecular proton transfer in hydroxyanthraquinones: Toward predicting fading of organic red colorants in art. Sci Adv 2019;5:eaaw5227. https://doi.org/10.1126/sciadv.aaw5227.

[33] Tissier R-C, Rigaud B, Thureau P, Jaber M, Ferré N. Stressing the differences in alizarin and purpurin dyes through UV- visible light absorption and 1H-NMR spectroscopies n.d.:10.

[34] Jacquemin D, Brémond E, Ciofini I, Adamo C. Impact of Vibronic Couplings on Perceived Colors: Two Anthraquinones as a Working Example. J Phys Chem Lett 2012;3:468–71. https://doi.org/10.1021/jz201552x.

[35] Di Tommaso S, Bousquet D, Moulin D, Baltenneck F, Riva P, David H, et al. Theoretical approaches for predicting the color of rigid dyes in solution. J Comput Chem 2017;38:998–1004. https://doi.org/10.1002/jcc.24774.

[36] Le Person A, Cornard J-P, Say-Liang-Fat S. Studies of the tautomeric forms of alizarin in the ground state by electronic spectroscopy combined with quantum chemical calculations. Chemical Physics Letters 2011;517:41–5. https://doi.org/10.1016/j.cplett.2011.10.015.

[37] Tirri B, Turelli M, Boissonnat G, Ciofini I, Adamo C. Protocols for the in-silico screening of the perceived color of industrial dyes: Anthraquinones and indigos as study cases. Dyes and Pigments 2023;208:110826. https://doi.org/10.1016/j.dyepig.2022.110826.

[38] Carta L, Biczysko M, Bloino J, Licari D, Barone V. Environmental and complexation effects on the structures and spectroscopic signatures of organic pigments relevant to cultural heritage: the case of alizarin and alizarin–Mg(ii)/Al(iii) complexes. Phys Chem Chem Phys 2014;16:2897. https://doi.org/10.1039/c3cp50499a.

[39] Pedone A, Biczysko M, Barone V. Environmental Effects in Computational Spectroscopy: Accuracy and Interpretation. ChemPhysChem 2010;11:1812–32. https://doi.org/10.1002/cphc.200900976.

[40] Miliani C, Romani A, Favaro G. Acidichromic effects in 1,2-di- and 1,2,4-tri- hydroxyanthraquinones. A spectrophotometric and fluorimetric study. Journal of Physical Organic Chemistry 2000;13:141–50. https://doi.org/10.1002/(SICI)1099-1395(200003)13:3<141::AID-POC220>3.0.CO;2-J.

[41] Shalaby AA, Mohamed AA. Determination of acid dissociation constants of Alizarin Red S, Methyl Orange, Bromothymol Blue and Bromophenol Blue using a digital camera. RSC Adv 2020;10:11311–6. https://doi.org/10.1039/C9RA10568A.

[42] Software update: The ORCA program system—Version 5.0 - Neese - 2022 - WIREs Computational Molecular Science - Wiley Online Library n.d. https://wires.onlinelibrary.wiley.com/doi/full/10.1002/wcms.1606 (accessed August 24, 2023).

[43] Bannwarth C, Ehlert S, Grimme S. GFN2-xTB—An Accurate and Broadly Parametrized Self-Consistent Tight-Binding Quantum Chemical Method with Multipole Electrostatics and Density-Dependent Dispersion Contributions. J Chem Theory Comput 2019;15:1652–71. https://doi.org/10.1021/acs.jctc.8b01176.

[44] Parr RG, Weitao Y. Density-Functional Theory of Atoms and Molecules. Oxford University Press; 1994.

[45] Marques MAL, Maitra NT, Nogueira FMS, Gross EKU, Rubio A. Fundamentals of time-dependent density functional theory. Fundamentals of Time-Dependent Density Functional Theory, 2012, p. 1–559.

[46] Adamo C, Barone V. Toward reliable density functional methods without adjustable parameters: The PBE0 model. The Journal of Chemical Physics 1999;110:6158–70. https://doi.org/10.1063/1.478522.

[47] Effect of the damping function in dispersion corrected density functional theory - Grimme - 2011 - Journal of Computational Chemistry - Wiley Online Library n.d. https://onlinelibrary.wiley.com/doi/10.1002/jcc.21759 (accessed December 3, 2023).

[48] Becke AD, Johnson ER. A density-functional model of the dispersion interaction. J Chem Phys 2005;123:154101. https://doi.org/10.1063/1.2065267.

[49] A consistent and accurate ab initio parametrization of density functional dispersion correction (DFT-D) for the 94 elements H-Pu | The Journal of Chemical Physics | AIP Publishing n.d. https://pubs.aip.org/aip/jcp/article-abstract/132/15/154104/926936/A-consistent-and-accurate-ab-initio?redirectedFrom=fulltext (accessed December 3, 2023).

[50] Weigend F, Ahlrichs R. Balanced basis sets of split valence, triple zeta valence and quadruple zeta valence quality for H to Rn: Design and assessment of accuracy. Phys Chem Chem Phys 2005;7:3297–305. https://doi.org/10.1039/B508541A.

[51] Pracht P, Bohle F, Grimme S. Automated exploration of the low-energy chemical space with fast quantum chemical methods. Phys Chem Chem Phys 2020;22:7169–92. https://doi.org/10.1039/C9CP06869D.

[52] Liakos DG, Guo Y, Neese F. Comprehensive Benchmark Results for the Domain Based Local Pair Natural Orbital Coupled Cluster Method (DLPNO-CCSD(T)) for Closed- and Open-Shell Systems. J Phys Chem A 2020;124:90–100. https://doi.org/10.1021/acs.jpca.9b05734.

[53] Garcia-Ratés M, Neese F. Efficient implementation of the analytical second derivatives of hartree–fock and hybrid DFT energies within the framework of the conductor-like polarizable continuum model. Journal of Computational Chemistry 2019;40:1816–28. https://doi.org/10.1002/jcc.25833.

[54] Warshel A, Levitt M. Theoretical studies of enzymic reactions: Dielectric, electrostatic and steric stabilization of the carbonium ion in the reaction of lysozyme. Journal of Molecular Biology 1976;103:227–49. https://doi.org/10.1016/0022-2836(76)90311-9.

[55] Groenhof G. Introduction to QM/MM Simulations. In: Monticelli L, Salonen E, editors. Biomolecular Simulations: Methods and Protocols, Totowa, NJ: Humana Press; 2013, p. 43–66. https://doi.org/10.1007/978-1-62703-017-5_3.

[56] Senn HM, Thiel W. QM/MM Methods for Biomolecular Systems. Angewandte Chemie International Edition 2009;48:1198–229. https://doi.org/10.1002/anie.200802019.

[57] Neese F, Wennmohs F, Becker U, Riplinger C. The ORCA quantum chemistry program package. The Journal of Chemical Physics 2020;152:224108. https://doi.org/10.1063/5.0004608.

[58] Martyna GJ, Tuckerman ME, Tobias DJ, Klein ML. Explicit reversible integrators for extended systems dynamics. Molecular Physics 1996;87:1117–57. https://doi.org/10.1080/00268979600100761.

[59] Jacquemin D, Wathelet V, Perpète EA, Adamo C. Extensive TD-DFT Benchmark: Singlet-Excited States of Organic Molecules. J Chem Theory Comput 2009;5:2420–35. https://doi.org/10.1021/ct900298e.

[60] Becke AD. Density-functional thermochemistry. III. The role of exact exchange. The Journal of Chemical Physics 1993;98:5648–52. https://doi.org/10.1063/1.464913.

[61] Laurent AD, Jacquemin D. TD-DFT benchmarks: A review. International Journal of Quantum Chemistry 2013;113:2019–39. https://doi.org/10.1002/qua.24438.

[62] Jacquemin D, Mennucci B, Adamo C. Excited-state calculations with TD-DFT: from benchmarks to simulations in complex environments. Phys Chem Chem Phys 2011;13:16987. https://doi.org/10.1039/c1cp22144b.

[63] Orlandi G, Siebrand W. Theory of vibronic intensity borrowing. Comparison of Herzberg-Teller and Born-Oppenheimer coupling. The Journal of Chemical Physics 2003;58:4513–23. https://doi.org/10.1063/1.1679014.

[64] Small GJ. Herzberg–Teller Vibronic Coupling and the Duschinsky Effect. The Journal of Chemical Physics 2003;54:3300–6. https://doi.org/10.1063/1.1675343.

[65] Sussmann R, Neuhauser R, Neusser HJ. High-resolution UV spectroscopy of vibronic bands in p-difluorobenzene and p-difluorobenzene–Ar: The role of Herzberg–Teller coupling. Can J Phys 1994;72:1179–86. https://doi.org/10.1139/p94-151.

[66] de Souza B, Neese F, Izsák R. On the theoretical prediction of fluorescence rates from first principles using the path integral approach. The Journal of Chemical Physics 2018;148:034104. https://doi.org/10.1063/1.5010895.

[67] Santoro F, Jacquemin D. Going beyond the vertical approximation with time-dependent density functional theory. WIREs Computational Molecular Science 2016;6:460–86. https://doi.org/10.1002/wcms.1260.

[68] Johnston-Feller R. Color science in the examination of museum objects: Nondestructive procedures. Color Research & Application 2002;27:456–7. https://doi.org/10.1002/col.10107.

[69] Colorimetry — Part 4: CIE 1976 L*a*b* colour space | CIE n.d. https://cie.co.at/publications/colorimetry-part-4-cie-1976-lab-colour-space-1 (accessed January 29, 2024).

[70] Karma IGM. Determination and Measurement of Color Dissimilarity. International Journal of Engineering and Emerging Technology 2020;5:67. https://doi.org/10.24843/IJEET.2020.v05.i01.p13.

[71] Mokrzycki W, Tatol M. Color difference Delta E - A survey. Machine Graphics and Vision 2011;20:383–411.

[72] Habekost M. Which color differencing equation should be used? 2013.

[73] Santra G, Martin JML. Pure and Hybrid SCAN, rSCAN, and r2SCAN: Which One Is Preferred in KS- and HF-DFT Calculations, and How Does D4 Dispersion Correction Affect This Ranking? Molecules 2022;27:141. https://doi.org/10.3390/molecules27010141.

[74] de Oliveira MT, Alves JMA, Braga AAC, Wilson DJD, Barboza CA. Do Double-Hybrid Exchange–Correlation Functionals Provide Accurate Chemical Shifts? A Benchmark Assessment for Proton NMR. J Chem Theory Comput 2021;17:6876–85. https://doi.org/10.1021/acs.jctc.1c00604.

[75] Jensen F. Segmented Contracted Basis Sets Optimized for Nuclear Magnetic Shielding. J Chem Theory Comput 2015;11:132–8. https://doi.org/10.1021/ct5009526.

[76] Preat J, Laurent AD, Michaux C, Perpète EA, Jacquemin D. Impact of tautomers on the absorption spectra of neutral and anionic alizarin and quinizarin dyes. Journal of Molecular Structure: THEOCHEM 2009;901:24–30. https://doi.org/10.1016/j.theochem.2008.12.032.

[77] Giovannini T, Egidi F, Cappelli C. Molecular spectroscopy of aqueous solutions: a theoretical perspective. Chem Soc Rev 2020;49:5664–77. https://doi.org/10.1039/C9CS00464E.